2013

Coupled Continuum and Molecular Model of Flow through Fibrous Filter

Shunliu Zhao
University of Akron, main campus

Alex Povitsky
University of Akron, main campus

Coupled continuum and molecular model of flow through fibrous filter

Shunliu Zhao and Alex Povitsky

Citation: Physics of Fluids (1994-present) **25**, 112002 (2013); doi: 10.1063/1.4830315
View online: http://dx.doi.org/10.1063/1.4830315
View Table of Contents: http://scitation.aip.org/content/aip/journal/pof2/25/11?ver=pdfcov
Published by the AIP Publishing

PHYSICS OF FLUIDS **25**, 112002 (2013)

Coupled continuum and molecular model of flow through fibrous filter

Shunliu Zhao and Alex Povitsky
Department of Mechanical Engineering, The University of Akron, Akron, Ohio 44325-3903, USA

(Received 22 October 2012; accepted 20 October 2013; published online 18 November 2013)

A coupled approach combining the continuum boundary singularity method (BSM) and the molecular direct simulation Monte Carlo (DSMC) is developed and validated using Taylor-Couette flow and the flow about a single fiber confined between two parallel walls. In the proposed approach, the DSMC is applied to an annular region enclosing the fiber and the BSM is employed in the entire flow domain. The parameters used in the DSMC and the coupling procedure, such as the number of simulated particles, the cell size, and the size of the coupling zone are determined by inspecting the accuracy of pressure drop obtained for the range of Knudsen numbers between zero and unity. The developed approach is used to study flowfield of fibrous filtration flows. It is observed that in the partial-slip flow regime, $Kn \leq 0.25$, the results obtained by the proposed coupled BSM-DSMC method match the solution by BSM combined with the heuristic partial-slip boundary conditions. For transition molecular-to-continuum Knudsen numbers, $0.25 < Kn \leq 1$, the difference in pressure drop and velocity between these two approaches is significant. This difference increases with the Knudsen number that confirms the usefulness of coupled continuum and molecular methods in numerical modeling of transition low Reynolds number flows in fibrous filters. [http://dx.doi.org/10.1063/1.4830315]

I. INTRODUCTION

Fibrous filters are used to separate liquid and solid particles as well as live objects from gas and liquid flows. Integral performance of filters has been evaluated in terms of capturing efficiency and pressure drop.[1,2] So-called cell models for predicting the capturing efficiency and/or pressure drop of fibrous media were developed for the continuum no-slip and partial-slip flow regimes.[1,3–7] Nevertheless, detailed models of flow field in filters are needed, for example, to predict the position of the adsorbed particles within the multi-diameter non-structured fiber web.[8] A detailed model of flow field is important to predict fouling and caking that can render the filter ineffective.[9] In order to group particles according to their size range, a promising lateral displacement technique with staggered fibers[10,11] need to be modeled to ensure separation of particles by their flow paths. Development of these models is especially important in transitional continuum to molecular flow regime, in which neither continuum nor free molecular flow field assumptions are valid.

The setup of the fiber filtration problem considered in the current study is shown in Fig. 1. A similar setup of fibers has been used for experimental studies of filtration flows.[12] Quantitative values of parameters of multi-fiber setup shown in Fig. 1 including packing factor of fibers, α, are presented in Sec. IV A.

Most of prior studies regarding filtration gas flows in the continuum regime assume no-slip boundary conditions (BC) that correspond to $Kn \leq 0.01$. Here, Kn is the Knudsen number defined as the ratio of molecular mean-free path to the fiber radius.[1,13] Recent practical interest to capturing micrometer and nano-meter scale particles calls for investigation of higher Kn numbers flows in filtration setting. This study is focused on the development of combined continuum approach based on boundary singularity method (BSM) and molecular approach to flows with Knudsen numbers $0.01 \leq Kn \leq 1$, and to analysis of flows about single and multiple fibers using the developed

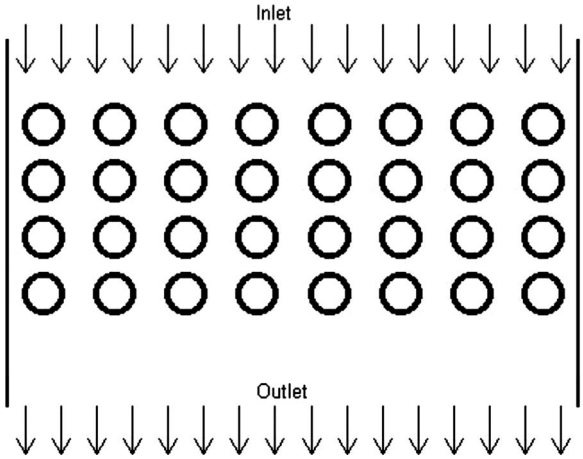

FIG. 1. Schematic for the flow in a filter with representative 4 × 8 set of cylindrical fibers.

methodology. Typical filter geometry (Fig. 1) has relatively low packing factor of fibers and the size of filter is of order of magnitude larger than the fiber radius (see Sec. IV A for details). While the value of *Kn* based on fiber radius can be of order of unity, the value of *Kn* based on filter size is of order of magnitude smaller. The goal of the current study is to develop and apply methodology that combines molecular approach at individual fibers' scale and continuum approach at the filter scale.

The coupling technique of continuum BSM and molecular Direct Simulation Monte Carlo (DSMC) will be proposed and validated for $Kn \leq 1$ using test cases such as the Taylor-Couette flow between two cylinders and flow about single fiber in confined space and then applied to study flows about sets of fibers. Parameters of the coupling scheme including the thickness of the interface zone, needed number of couplings between BSM and DSMC and the number of simulated particles will be established by numerical experiments.

For micro-scale fibrous filters, the flow is usually considered as incompressible due to the low pressure drop across a filter. The associated Reynolds number based on fiber diameter is commonly below unity so that the Stokes approximation can be used for filtration flows.[1] The efficient technique to solve the Stokes equations in arbitrary complex geometry is the BSM, which does not require meshing of flow domain but only need to place the BSM singularities at the domain boundaries. The BSM has been successfully applied to a number of two- and three-dimensional Stokes flows in the continuum flow regime, such as cavity flows,[14] flows caused by the motion of solid particles,[15,16] spiral swimming flows,[17,18] and movement of spherical particles in capillaries.[19] In recent papers by Zhao and Povitsky,[20–22] the BSM has been extended to two- and three-dimensional partial-slip flows and successfully applied to fibrous filtration flows in partial-slip regime.[22]

For micro- and nano- flows, the continuum hypothesis and assumption of no-slip boundary condition are no longer valid near solid fibers.[13] Efforts have been made to model flows at $Kn > 0.01$ by using the DSMC and Molecular Dynamics (MD) approaches. The deterministic MD method is valid in principle for all the flow regimes. However, the MD is extremely computationally expensive since it involves all molecular and atomic interactions of molecules in considered computational domain. Thus, this study adopts the computationally efficient DSMC, a stochastic approach for molecular-level modeling of gas flows.

The DSMC method, first developed for rarefied gas flows,[23,24] is a particle simulation method based on kinetic theory. The DSMC solves the dynamics of ensemble of molecules by tracking a representative set of particles, where each simulated particle represents millions of molecules.[23,25] In frame of DSMC, the particles motions are modeled deterministically, while the collisions among molecules are treated statistically as collisions between representative particles. The DSMC has been used widely and successfully in high-speed flow simulations for rarefied gas flow applications.[23,26] It also has been used to model micro-scale slider air bearing problems.[27,28]

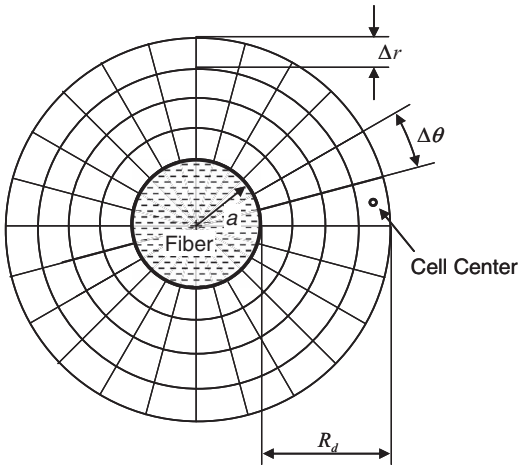

FIG. 2. DSMC sub-domain and DSMC cells.

The DSMC is very computationally intensive compared to the solution of continuum conservation laws equations. Coupled continuum and molecular modeling require less computational resources and are still accurate when the modeled flow domain can be split on continuum and rarefied sub-domains.[29–32] Various hybrid methods have been developed for steady and unsteady flows, which includes the Navier-Stokes equations coupled with the DSMC method[29] or Boltzmann equations,[33] the Euler equations coupled with the DSMC,[32] and the Stokes equations combined with the DSMC.[31] In the above references, finite volume discretization techniques were used for continuum equations whereas the boundary singularity method has not been combined yet with molecular approach. The advantages of boundary singularity method compared to finite volume discretization and reduction in number of grid nodes and easiness of grid generation limited to surface of fibers. These advantages are important for fiber filters with irregular and/or dynamically adjusting fiber structure with varying diameters of fibers because finite-volume mesh generation is very difficult in these cases.

Accurate description of boundary conditions for flow about micro- and nano- fibers calls for molecular level model of slipping layer of fluid surrounding fibers. In the proposed approach, the DSMC is used in the sub-domain adjacent to fiber and the entire domain is presented by the continuum BSM (see Fig. 2). The cylindrical DSMC area encompasses each individual fiber and does need to conform to the bounding geometry of filter. At the interface between the molecular and continuum models, fluid flow variables or fluxes of mass, momentum, and energy should be matched to link the continuum and molecular models. Different coupling strategies have been employed in literature, such as a weakly coupled scheme, for which a continuum solution on the entire computational domain provides a boundary condition for a particle method, and overlapping coupling, for which a local molecular method provides a boundary condition for a global continuum scheme.[34] However, the coupling of molecular and boundary singularity methods has not been proposed yet that limits the application of BSM to transition continuum-molecular flows. In the current study, a coupled method of BSM and DSMC is developed and applied to filtration flows in the transition flow regime.

In literature, the major coupling problem was matching pressure between molecular and continuum solvers.[31] The proposed BSM-DSMC does not need to couple pressure explicitly because the linear system (1) for unknown strength of Stokeslets has velocities at collocation points at solid-fluid boundary in the right-hand side while pressure is not included in system (1). In the current study, the coupling between BSM and DSMC is established by values of velocities. This coupling procedure will be validated in terms of convergence to known solutions, accuracy, and absence on non-physical solution oscillations. Parameters of the coupled method are selected to minimize needed computational resources.

Using the developed coupled BSM-DSMC procedure, the pressure and velocity field will be obtained for partial slip and transition regimes for filter shown in Fig. 1. The difference in

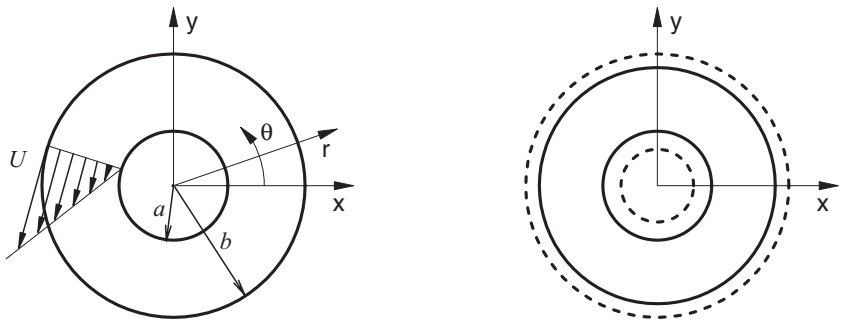

FIG. 3. Taylor-Couette flow: (a) flow schematic and (b) location of Stokeslets (dashed lines) for BSM.

computational results between the proposed coupled BSM-DSMC and BSM with heuristic partial slip boundary conditions will be evaluated as a function of Knudsen number.

The paper is set up as follows. In Sec. II, the BSM and DSMC procedures are outlined and applied as two isolated methods to the Taylor-Couette flow in the partial-slip regime. Solutions obtained by BSM and DSMC will be compared to analytical solution of the Taylor-Couette flow. In Sec. III, the coupled method of BSM and DSMC is proposed. The proposed method is implemented and validated using flow about a single fiber in confined space. The governing parameters for the DSMC and for the coupling procedure are obtained to ensure numerical stability, convergence, and accuracy. In Sec. IV, flows through set of fibers (Fig. 1) are studied by applying the coupled method. Computational savings are estimated as a function of parameters of filter and flow.

II. CONTINUUM AND MOLECULAR METHODS USED

In this section, the BSM and DSMC procedures are introduced and validated using analytical solution for steady two-dimensional Taylor-Couette flow between two infinite concentric cylinders. For Taylor-Couette flow (Fig. 3(a)), the inner cylinder is at rest and the outer one rotates at a given speed. The BSM and the DSMC are applied separately to solve the Taylor-Couette flow in the partial slip flow regime. A good agreement is observed between the numerical results obtained by these two methods and analytical solution of Taylor-Couette flow.

A. Boundary singularity method

The BSM solution is obtained by superposing the fundamental solutions to the Stokes equations. In this study, Stokeslets are taken as fundamental solutions. The unknown strength of Stokeslets is obtained by solving a system of linear equations formed by enforcing the solution to satisfy boundary conditions at collocation points located at fibers' surface.[35] Unlike other boundary element methods, which are based on the integral representations of governing equations and require a continuous surface distribution of singularities and the computation of the singular single-layer and double-layer integrals, the BSM involves only a point-wise distribution of singularities and thus simplifies the computations. A systematic study of the BSM for two- and three-dimensional partial slip flows was presented in Refs. 20–22.

For two-dimensional Stokes flows, the governing equation for a set of Stokeslets with unknown strengths[36] is given as

$$u_j^{(k)} = \frac{1}{4\pi\mu}\sum_{i=1}^{N}\left(F_i^{(k)}\ln|\vec{r}_{ij}| - \frac{F_i^{(m)}r_{ij}^{(m)}}{|\vec{r}_{ij}|^2}r_{ij}^{(k)}\right), \tag{1}$$

where $\vec{F}$ $(F^{(1)}, F^{(2)})$ is the Stokeslet composed of scalar components $F^{(1)}$ and $F^{(2)}$, μ is the fluid viscosity, $k = 1,2$ in two-dimensional cases, $\vec{r}_{ij} = (x_j - x_i, y_j - y_i)$ is the vector directed

from the Stokeslet to the collocation point located at boundary, and $|\vec{r}_{ij}|$ is the distance between the collocation point, j, and the Stokeslet, i. The Einstein summation rule applies to superscript $m = 1, 2$.

The pressure field induced by a single Stokeslet, i, can be expressed as

$$p = -\frac{1}{2\pi}\frac{F^{(i)}r^{(i)}}{|\vec{r}|^2}. \tag{2}$$

The pressure at a point caused by superposition of N Stokeslets can be expressed as summation in the right-hand sides of Eq. (2) corresponding to individual Stokeslets.

In the partial slip flow regime, a so-called Knudsen molecular layer (layer of fluid slipping with respect to the solid boundary) near solid-fluid interfaces is formed. The velocity field within the narrow Knudsen layer cannot be analyzed using the continuum Stokes equations or Navier-Stokes equations. However, heuristic slip models such as Maxwell's first-order velocity slip can be used at relatively low values of the Kn number. This helps to avoid computationally expensive solution of molecular-level equations such as Boltzmann equation. Partial-slip and no-penetrating BC at the rigid surfaces in the cylindrical coordinate system are given as

$$\begin{cases} u_\theta = u_{s\theta} + c\left(\frac{\partial u_\theta}{\partial r}\right)_{r=a} \\ u_r = u_{sr} \end{cases}, \tag{3}$$

where $c = Kn\ a$ is the coefficient determining the degree of partial slip in the boundary condition, Kn is the Knudsen number, a is the radius of cylinder, $u_{s\theta}$ and u_{sr} are the θ and r components of the solid boundary velocity. Fully diffuse reflection of gas molecules at wall (tangential momentum accommodation coefficient is equal to unity) is assumed in the current study. Velocity components $u_{s\theta}$ and u_{sr} are equal to zero for stationary rigid surfaces assumed in this study. In the limit case $Kn = 0$ and $c = 0$, the partial-slip BC (3) reduce to no-slip BC.

The solution procedure to find flow field by BSM is described as follows: by substituting derivatives of velocity (see Eq. (1) for velocity) into boundary conditions (3), a system of linear equations is formed. The strength of the Stokeslets $\vec{F}_i$ is obtained by solving this system. The velocity and pressure in the flow domain is then calculated straightforwardly by using Eqs. (1) and (2) with corresponding values of vectors r, directed from Stokeslets to any point in the flow domain. See Refs. 20–22 for details.

B. Direct simulation Monte Carlo method

In the DSMC, the real molecules are represented by a much smaller amount of simulated particles. The adopted DSMC consists of five steps:[23] (1) initialization; (2) computation displacement of simulated particles after time step Δt; (3) indexing and cross-referencing simulated particles; (4) prediction of after-collision velocities of simulated particles; and (5) sampling the simulated particles to obtain macroscopic properties of the flow.

The first step is the initialization procedure, which defines fluid properties, the cell size, the ratio of the number of simulated particles to that of real molecules, and the number of simulated particles per cell.

The properties of the gas used in the current study are presented in Table I. The number density $n = \frac{p}{\kappa T}$, where κ is the Boltzmann constant. The density ρ is then calculated as $\rho = nm$. The mean free path, λ is calculated by Ref. 23 as follows:

$$\lambda = \frac{1}{\sqrt{2}\pi d_{ref}^2 n \left(T_s / T_{ref}\right)^{\omega-\frac{1}{2}}}, \tag{4}$$

where T_s is the stream temperature. Values of parameters in the right-hand side of Eq. (4) are shown in Table I.

A sufficient number of simulated particles per computational cell must be maintained to ensure accuracy. The optimum number of simulated particles is a tradeoff between accuracy and

TABLE I. Gas properties for VHS at $T_{ref} = 273\,^{\circ}$C and $p = 1.01325 \times 10^5$. Here, m is the molecular mass, μ is viscosity, ω is viscosity-temperature power-law exponent, and d_{ref} is the reference molecular diameter.

m ($\times 10^{27}$ kg)	μ ($\times 10^5$ kg m^{-1}s^{-1})	ω	d_{ref} ($\times 10^{10}$ m)
46.5	1.80	0.74	4.17

computational cost. This number is problem-specific[27,37–42] and will be obtained for the cases considered in Secs. II C, III, and IV.

The number of simulated particles $n_p = \rho_p V_d$, where ρ_p is the density of the simulated particles and V_d is the volume of the DSMC sub-domain. The value of V_d is the product of the cross-sectional DSMC area (see Fig. 2), $\pi R_d(2a + R_d)$ and the length of the DSMC computational domain along fiber. In the current study, the fibers are assumed to be of infinite length, that is, end fiber effects are neglected. The length of the DSMC zone along fiber was set to be equal to the fiber radius, a. The number of simulated particles per cell is then determined by the cell size and ρ_p.

The discretization of the DSMC computational sub-domain is then performed (see Fig. 2). The cell size is set to be $\Delta r = C_c\lambda$, where the parameter C_c ranges from 0.1 to 0.9. The number of cells in the r direction is given by $N_r = R_d / \Delta r$. The number of cells in the θ direction is determined by the perimeter of the middle circle with its radius $a+R_d/2$ so as $N_\theta = 2\pi(a + \frac{R_d}{2}) / \Delta r$. Each cell is subdivided to the 2×2 grid of sub-cells.

The initial position and velocity of the simulated DSMC particles are assigned cell by cell. A simulated particle is randomly located within the cell to which it was assigned. The initial velocity distribution is taken as the Maxwell velocity distribution.[23]

The second DSMC step is the tracking of motion of simulated particles, which determines the new locations of the simulated particles after a time step deterministically. The time step $\Delta t = 0.25\Delta r / c'_m$, where c'_m is the most probable molecular speed. The time step is chosen so that it would take a typical particle with the most probable speed several time steps to traverse a cell.[28,43]

At this step, the interactions of simulated particles with walls and the entrance/exit boundary conditions must be considered. The diffuse reflection model is used in the current study. The diffuse reflection model is a fair approximation if the solid surface is not precisely processed and is maintained at room temperature.[44] The particle's velocity after collision with domain boundary is reset randomly by a biased Maxwellian distribution.[23]

When a simulated particle hits a wall, the computational procedure is set up as follows: first, the interaction point at the wall is found; second, the time for the simulated particle to reach the interaction point, $\Delta t'$, is calculated; third, the new velocity components after reflection are computed; finally, the new location of the simulated particle after traveling with the new velocity during the time interval $(\Delta t - \Delta t')$ is obtained.

The boundary conditions need to be enforced if the new location of a simulated particle is out of the computational domain. When a particle leaves the DSMC domain, a new particle is generated and enters a cell randomly selected from the cells along the boundary through which the previous particle exits.

The third DSMC step is to index and cross-reference the particles. At the end of each time step, a simulated particle might not be in the same sub-cell or cell. Particles' collisions are calculated cell by cell; therefore, the cross-referencing process is needed to indicate which particles are contained in a cell. The DSMC requires indexing to indicate the cell to which a particle does belong.

The fourth DSMC step is modeling the collisions of simulated particle, which is a statistical procedure. The time-counter (TC) method for the particle collision procedure was introduced in Ref. 23, which has a computation time directly proportional to the square of the total number of particles. To improve the efficiency of the TC method, a number of schemes were proposed[23,45,46] including the no-time-counter method (NTC)[47] which has a computational time proportional to the total number of particles.

The NTC procedure is adopted in the current study to obtain post-collision DSMC velocities. The NTC procedure is used together with the sub-cell technique. The sub-cell method further restricts particle collisions from cell to sub-cell to improve accuracy without significant computational cost. To determine the post-collision velocities of two simulated particles, a number of models have been proposed.[23] The Variable Hard Sphere (VHS) model includes the potential force of the inverse power law so that the collision cross-section varies with the relative velocity of two particles.[44] The VHS model removes deficiency in the basic hard sphere model and retains the simplicity of implementation.[13]

The last main DSMC step is the sampling of the flow field to obtain the representative macroscopic properties at the center of each cell. For steady flows, the sampling process usually starts after thousands time steps to ensure that the flow reaches the steady state.[42] The flow properties are sampled for each cell every several time steps and the desired steady result is a time average of all the sampled values. In the current study, the sampling process starts after 2000 time steps and does the sampling every two time steps thereafter. The sampling process continues until a prescribed tolerance is reached.

C. BSM and DSMC for low-Reynolds-number Taylor-Couette flow

The flow confined in the gap between two concentric rotating cylinders is solved numerically by continuum BSM and by molecular DSMC to illustrate the applicability of the components of proposed methodology to partial-slip interior flows. The inner cylinder is at rest and the outer cylinder rotates counter-clockwise with the tangential rotational velocity equal to U (see Fig. 3(a)). The center of the two concentric cylinders is located at the origin.

The analytical solution of the considered Taylor-Couette flow can be written as

$$u_\theta = Ar + \frac{B}{r}, \tag{5}$$

where

$$A = \frac{U(a+2c)b^2}{ab(b^2-a^2)+2c(b^3+a^3)},$$

$$B = -\frac{Ua^3b^2}{ab(b^2-a^2)+2c(b^3+a^3)},$$

a is the radius of the inner cylinder, b is the radius of the outer cylinder, and $c = aKn$ (Eq. (3)) is the slip coefficient. For no-slip flows, $c = 0$ and the coefficients A and B reduce to the ones presented in Ref. 48. For $a = 1$, the value of parameter c is equal to Kn. In the current computations, the thickness of the annulus between the two cylinders ($a = 1$ and $b = 1.4$) is equal to 0.4, the mean free path $\lambda = 0.04$, and therefore, $Kn = 0.1$. For instance, the value of slip velocity at inner cylinder surface computed by above formulae is 0.187.

In the BSM computations, Stokeslets are located outside the flow domain (see Fig. 3(b)) to avoid singularities at collocation points.[22] The number of Stokeslets used for the inner cylinder is equal to 20. For the outer cylinder, the number of Stokeslets is approximately equal to $28 = 20b/a$. The radii of circles, at which Stokeslets located, are $0.8a$ for the inner cylinder and $2.66b$ for the outer cylinder (see Fig. 3(b)).

The DSMC procedure for the considered Taylor-Couette flow is tested by varying the number of simulated particles per cell and cell size. It is shown in Fig. 4(a) that 7.5 simulated particles per cell of the size of 0.5λ is sufficient. Fig. 4(b) indicates that the cell size could vary from 0.3λ to 0.9λ without substantially alternating DSMC results. Fig. 4(c) presents numerical results obtained from BSM and DSMC for $Kn = 0.1$. If $n_p = 7.5$, the BSM and DSMC results agree well with the analytical solution of the Taylor-Couette flow presented above (see Fig. 4(c)).

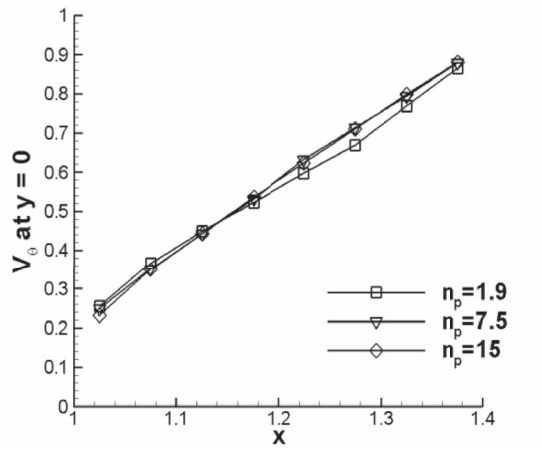

(a)

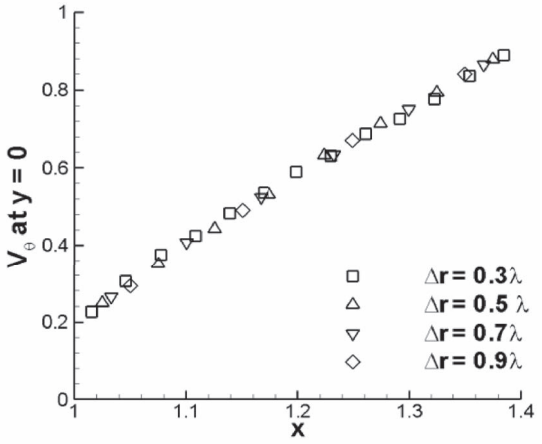

(b)

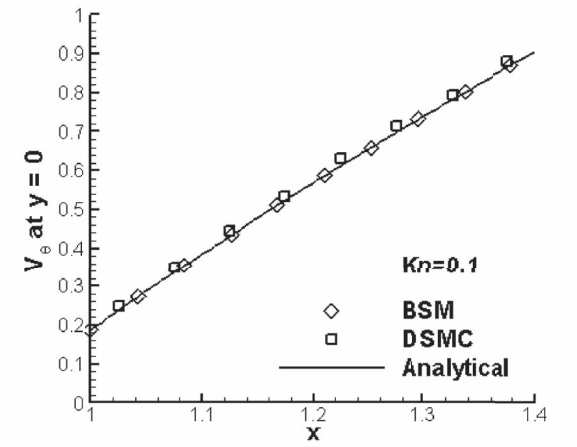

(c)

FIG. 4. DSMC results for the Taylor-Couette flow at $Kn = 0.1$. The θ component of velocity between the inner and outer cylinders is shown at $y = 0$ when $1 < x < 1.4$: (a) velocity profile for the number of simulated particles per cell, $n_p = 1.9$, 7.5, and 15; the cell size 0.5λ; (b) velocity profile for the range of cell sizes; and (c) comparison of velocity profiles obtained by BSM, DSMC, and by analytical Eq. (5).

III. COUPLING OF BSM AND DSMC AND APPLICATION OF COUPLED BSM-DSMC TO FLOW ABOUT A FIBER

In this section, the hybrid method of BSM and DSMC is proposed and validated using flow about a single fiber in confined space as a benchmark. Since the BSM is established and validated in Sec. II A, the numerical results by hybrid BSM-DSMC are compared with those obtained by BSM with partial-slip boundary conditions (3), which are adequate for Kn = 0.1.

A. The coupling of BSM and DSMC

The idea of the coupling is to use the DSMC method to generate more physically accurate boundary conditions for the BSM since the heuristic partial-slip boundary conditions are no longer valid for filtration flows in the transition regime ($Kn > 0.25$). For this purpose, the DSMC is applied to an annular region enclosing the cylinder (fiber) and the BSM is employed to the entire flow domain (see Fig. 5(a)). To initiate the coupling process, the BSM is used to provide the DSMC with

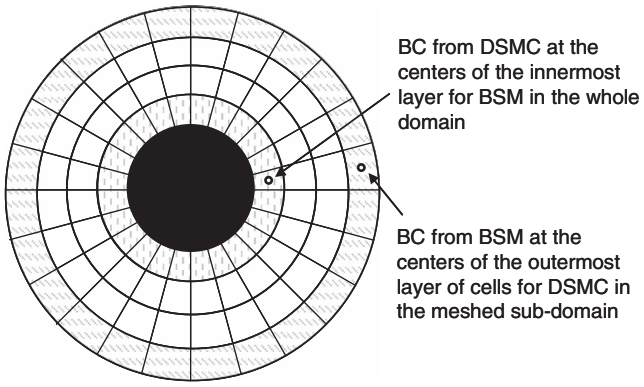

(a)

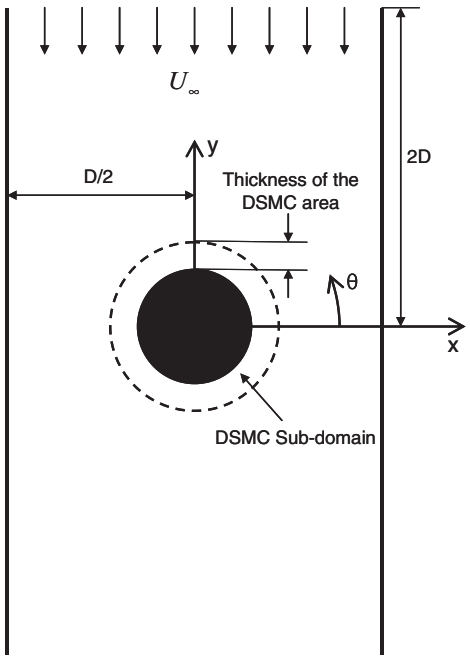

(b)

FIG. 5. Coupled BSM and DSMC method: (a) schematic for the BSM and DSMC exchange of boundary data and (b) the benchmark single fiber flow.

the boundary conditions at the outermost layer (the outer shadowed area in Fig. 5(a)). This approach represents a variant of the Schwarz alternating method to find the solution on a domain which is the union of two overlapping sub-domains. Matching of boundary conditions between molecular and continuum methods were employed by Refs. 49–51 in which for continuum sub-domain the Navier-Stokes finite-volume solver was used and for molecular sub-domain MD solver was adopted. Once the DSMC computations are completed, the velocities at the centers of the innermost layer of cells (the inner shadowed area in Fig. 5(a)) are used as the boundary conditions for the BSM. The BSM and DSMC are coupled after every BSM and DSMC iteration until a prescribed tolerance is reached.

At the outer boundary of DSMC domain, velocity field is assumed continuous and the DSMC velocity at the outer boundary is sampled stochastically around mean BSM velocity. As in Ref. 31, only Dirichlet–Dirichlet type boundary conditions are employed to avoid matching of estimated derivatives of flow quantities.

B. Application of coupled BSM-DSMC to flow about a fiber

A flow about a fiber confined with two parallel walls (see Fig. 5(b)) is used as the simplified model for multi-fiber fibrous filtration flows (see Fig. 1 and Sec. III C). The origin of the Cartesian coordinates is at the fiber center. The x axis is directed right and the y axis is directed upward. The distance between walls, $D = \sqrt{\pi / c_{pf}}a$ where $c_{pf} = 2.5\%$ is the packing factor. The value of packing factor is the same as that used in Sec. IV A for flow past multiple fibers.

The effect of the number density of simulated particles, thickness of the DSMC area, and the cell size on the pressure drop is investigated in this section. The proper values of these parameters are then chosen for computations of flow past multiple fibers in Sec. III C. Study of the slip velocity (Sec. III D) shows that in the transition flow regime ($Kn > 0.25$) the BSM with heuristic partial-slip boundary conditions are no longer accurate.

C. Selection of computational parameters of BSM-DSMC procedure

In this section, the computational parameters of combined BSM and DSMC are obtained as detailed below. The computational configuration is selected as follows: the thickness of the DSMC area is 3λ; the density of simulated particles $\rho_p = 3000$, corresponding to 7.5 simulated particles in a square cell with a size of 0.5λ.

With the other parameters unchanged, the pressure drop with respect to the number of coupling for various number densities of simulated particles is presented in Fig. 6(a). The pressure drop is calculated as $\Delta p = \bar{p}_2 - \bar{p}_1$, where cross-section averaged $\bar{p}_1$ and $\bar{p}_2$ are obtained at $y_1 = -D/2$ and $y_2 = D/2$, respectively. In Fig. 6, zero number of couplings corresponds to the results from pure BSM combined with the heuristic partial-slip boundary conditions.

It is found that the pressure drop obtained from the hybrid BSM-DSMC deviates no more than 2% from the one obtained by the BSM. This suggests that the BSM and the hybrid method agree well at $Kn = 0.1$. The pressure drop varies less than 2% with respect to the number of BSM-DSMC couplings (Fig. 6(b)).

The pressure drop after the third coupling with respect to ρ_p is shown in Fig. 6(c). Note that the case with $\rho_p = 1000$ corresponds to 2.5 simulated particle in a square cell with its size of 0.5λ. The graph is near-flat for $\rho_p \geq 1000$ that confirms that the pressure drop converges with ρ_p.

For $\rho_p = 3000$, the pressure drop variation is evaluated in terms of the size of the DSMC sub-domain and appears to be within 2% (see Fig. 6(c)). The results shown in Figs. 6(b) and 6(c) indicate that it would be sufficient to set the thickness of the DSMC sub-domain as three times the mean free path.

Having $\rho_p = 3000$ and the thickness of the DSMC area equal to 3λ, coupled BSM-DSMC computations are conducted to access the influence of cell size on pressure drop. The cell size is $\Delta r = C_c\lambda$, where C_c ranges from 0.1 to 0.9 with the increment of 0.2 and Δr is rounded to have integer N_r (see Table II). When the results are plotted, the actual value of Δr is used (see Table II and Fig. 6(d)). As shown in Fig. 6(d), when the pre-set $\Delta r = 0.1\lambda$, pressure drop deviates from those obtained from the previous calculations with bigger Δr (compare Figs. 6(a) and 6(d)). This is probably

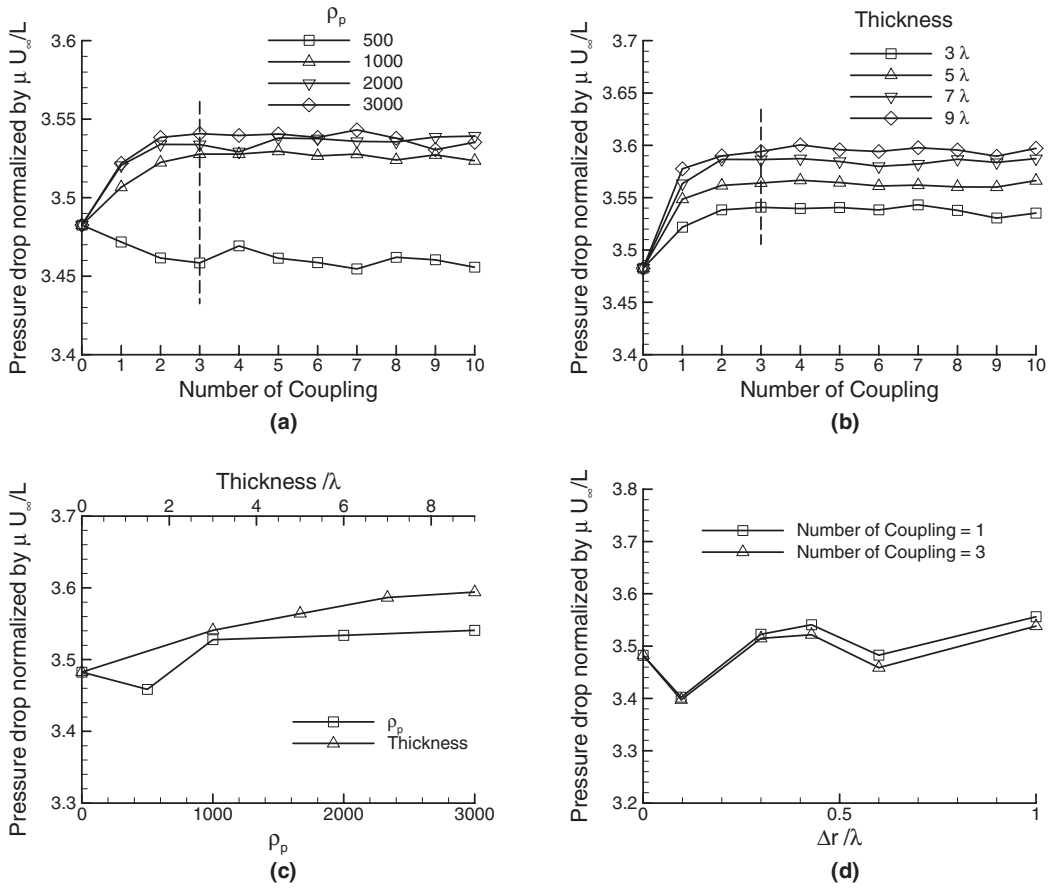

FIG. 6. Pressure drop for flow about a single fiber: (a) pressure drop with respect to the number of BSM-DSMC couplings for range of number densities of simulated DSMC particles; (b) pressure drop with respect to the number of coupling for range of thicknesses of the DSMC sub-domain; (c) pressure drop with respect to the number density and thickness of the DSMC sub-domain after the third BSM-DSMC coupling; and (d) pressure drop with respect to the cell size. Note: the zero value at the horizontal coordinate corresponds to the solution by the pure BSM combined with heuristic partial-slip boundary conditions (3).

caused by the insufficient number of particles in a cell. With a reduced number of particles in each cell, the sampled properties of particles might not be adequate to represent the macroscopic properties at the cell center. With the increase in cell size, the obtained pressure drop is almost constant until $\Delta r = 0.7\lambda$. Considering that the cell size suggested in Ref. 23 is less than mean free path λ and may be as low as 1/3 λ, the pre-set cell size is chosen to be 0.5λ.

D. Numerical results for flows about a single fiber at higher *Kn*

The coupled BSM-DSMC procedure with parameters chosen in Sec. III C is applied to flow about single fiber in transition molecular-to-continuum regime with Knudsen numbers of 0.5 and 1.0. The effects of number of couplings between DSMC and BSM and the size of DSMC zone are evaluated for these values of *Kn*.

TABLE II. The cell size (normalized by λ) and the number of particles per cell in a square cell with a size of the actual Δr.

Pre-set $\Delta r/\lambda$	0.1	0.3	0.5	0.7	0.9
Actual $\Delta r/\lambda$	0.097	0.30	0.43	0.60	1.0
n_p	0.28	2.7	5.5	11	30

TABLE III. The pressure drop after first two couplings of BSM and DSMC.

Kn	0.1	0.5	1.0
Δp after the first coupling	3.52	2.97	2.54
Δp after the second coupling	3.54	3.02	2.58
Difference in Δp between two couplings (%)	0.57	1.7	1.6

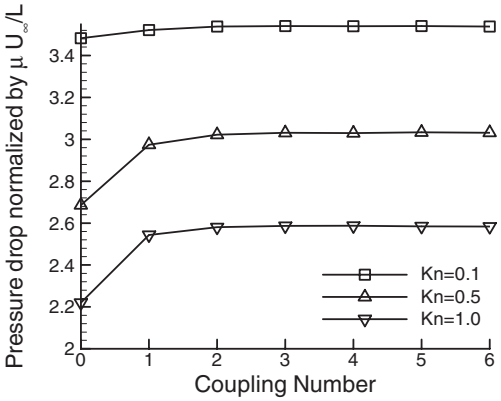

FIG. 7. Pressure drop for $Kn = 0.1$, 0.5, and 1.0 with respect to the number of couplings.

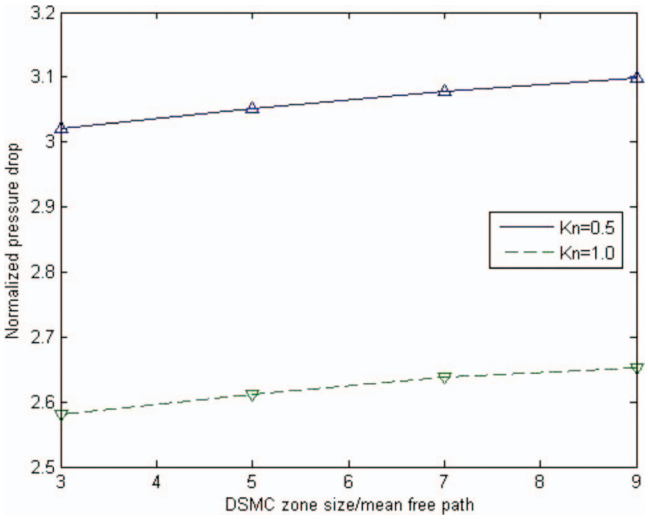

FIG. 8. Pressure drop for $Kn = 0.5$ and Kn = 1.0 with respect to the size of DSMC zone.

Fig. 7 presents the pressure drop with respect to the number of couplings for $Kn = 0.1$ (for comparison purpose), 0.5, and 1.0. The difference in pressure drop between the BSM and the coupled BSM-DSMC increases with the increase in Knudsen number. It is observed that the pressure drop has only minor variations after the first coupling for all the three Knudsen numbers considered. The change in pressure drop between the first coupling and the second one are shown in Table III. The difference between the pressure drop after the second coupling and the first one is below 2%. Thus, one coupling of BSM and DSMC is chosen for the following computations.

To evaluate the effect of the radius of DSMC zone for $Kn = 0.5$ and $Kn = 1.0$, the computations by the BSM-DSMC methods were conducted for the DSMC zone size ranging from 3λ to 9λ (see Fig. 8). Variations of pressure drop with the size of DSMC zone are comparable to that for $Kn = 0.1$ (see Figs. 6(b) and 6(c)), therefore, the DSMC zone radius of 3λ is used.

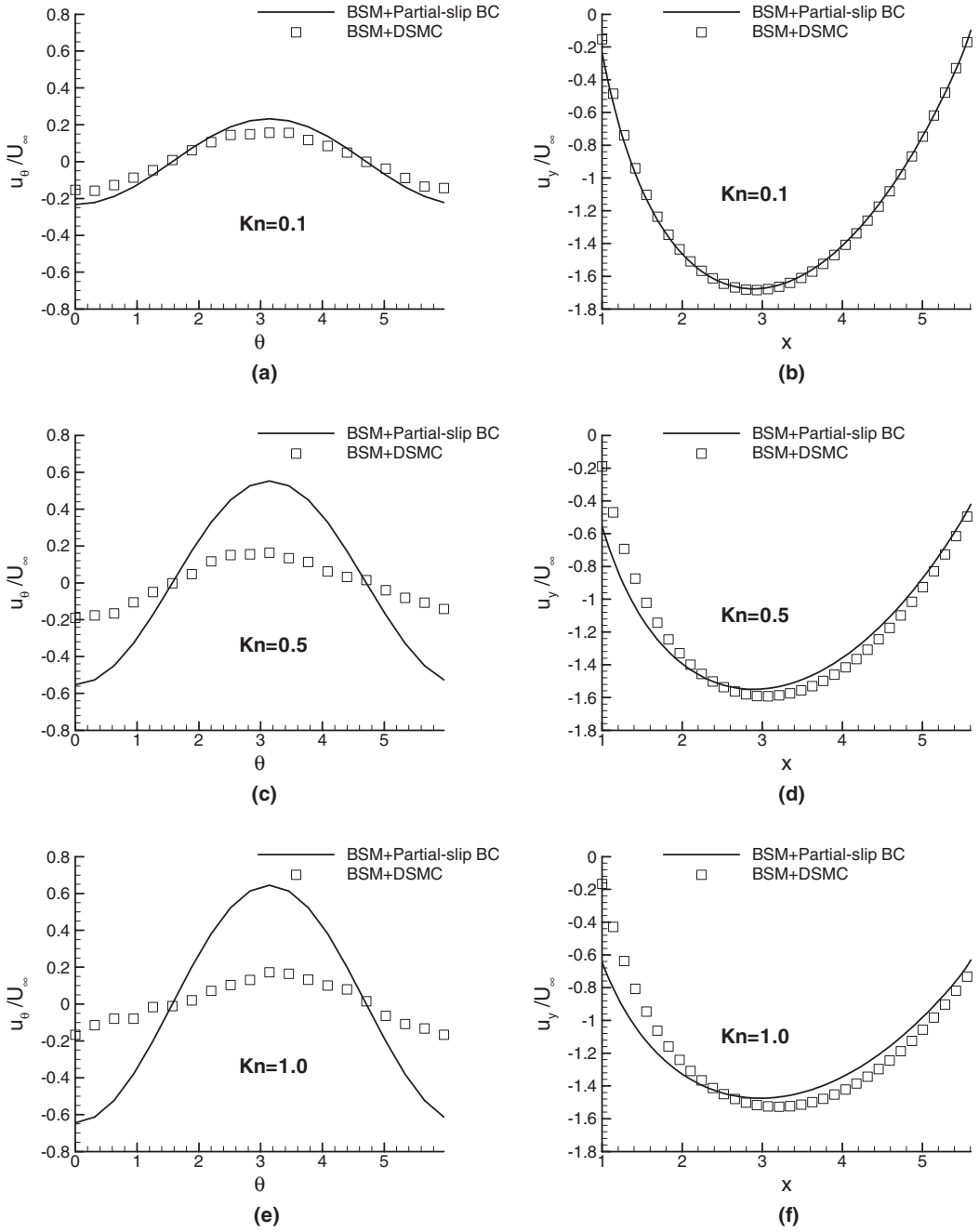

FIG. 9. Velocity profile for $Kn = 0.1$, 0.5, and 1.0: (a), (c), and (e) the tangential velocity along fiber surface; (b), (d), and (f) the y component of velocity along the x axis (at $y = 0$).

The profiles of velocity components for the BSM with heuristic partial slip boundary conditions (3) and the coupled BSM-DSMC are presented in Fig. 9. It is observed that the difference between velocity profiles obtained by the BSM and by the BSM-DSMC increases significantly with the increase in Knudsen number. The absolute value of the slip velocity predicted by the coupled method increases with the increase in the Knudsen number and is substantially lower than that obtained by the BSM with the first-order partial-slip heuristic boundary conditions (3). The difference in velocity obtained by these methods is not only noticeable at the fiber surface (Figs. 9(a), 9(c), and 9(e)), but also present in the flow domain farther from the fiber surface (Figs. 9(b), 9(d), and 9(f)).

IV. COUPLED BSM-DSMC APPLIED TO FLOW PAST MULTIPLE FIBERS

A. Setup of multiple fibers

The BSM-DSMC with parameters selected in Sec. III D is applied to multi-fiber problem depicted in Fig. 1, where a setup of 4 × 8 fibers is chosen and the packing factor is selected $c_{pf} = 2.5\%$ as in experiments.[12] The value of distance between centers of neighboring fibers α is calculated as $\alpha = \sqrt{\pi / c_{pf}} \approx 11.21$. The distance between the leftmost and rightmost columns of fibers and filter walls is selected as $\gamma = \alpha/2$. A similar geometry setup has been used for experiments[12] for no-slip filtration flows and numerical simulations of partial-slip filtration flows.[22]

For considered multi-fiber filtration, the pressure drop is calculated as $\Delta p = (\bar{p}_2 - \bar{p}_1)/(N_{row} - 2)$, where N_{row} is the number of rows of fibers, $\bar{p}_1$ and $\bar{p}_2$ are the average pressures at two horizontal cross-sections with their y coordinates y_1 and y_2, Here, $y = y_1$ is the cross-section in the middle between the bottom row of cylinders and the next-to-bottom row, and $y = y_2$ is the cross-section in the middle between the top row of cylinders and the next-to-top row.

The efficiency of coupled BSM-DSMC versus isolated DSMC for the entire multi-fiber problem is evaluated below. The computational time can be evaluated as being proportional to area covered by DSMC domain because the number of tracked DSMC particles is proportional to computational area and, by using NTC, the number of computed collisions is proportional to number of particles (see Sec. II B). By this estimate, computational time for the full DSMC is given by $T_o \sim \pi a^2(\frac{100}{C_{pf}} - 1)$, where πa^2 is the fiber cross-section, and C_{pf}, %, is a packing fraction. For the proposed coupled method with the thickness of DSMC zone equal to 3λ, the computational time $T \sim \pi((a + 3\lambda)^2 - a^2)$. The BSM takes only fraction of DSMC time and can be neglected in this estimate. Consequently, $T/T_o = (6Kn^2 + 9Kn^2)/(\frac{100}{C_{pf}} - 1)$. This ratio assumes that the convergence rate for pure DSMC is the same as that for smaller number of DSMC particles associated with the proposed method. Therefore, above evaluation is the lower bound of efficiency of the proposed BSM-DSMC. For $Kn = 1$ and $C_{pf} = 2.5\%$, this ratio is 2.6 while for $Kn = 0.5$ the ratio is 7.43. One can solve equation $T/T_o = 1$ to determine the critical value of Kn for a given C_{pf}.

Recall that the BSM does not require volume grid generation. Use of DSMC at near-fiber area requires simple cylindrical DSMC cells (see Fig. 2). Thus, time-consuming grid generation process for multi-fiber geometry is avoided by using proposed BSM-DSMC.

In a more broad sense, for multi-diameter micro- and nano-fiber filters only small fraction of domain surrounding nano-fibers need to be computed by DSMC so the proposed method is much more efficient than the full DSMC. Furthermore, the combination of DSMC and BSM is applicable

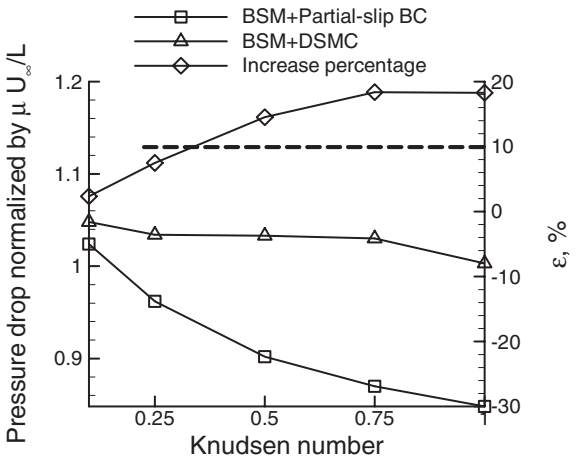

FIG. 10. Pressure drop for 4 × 8 set of fibers with respect to the Knudsen number. Here, ε is the relative pressure drop difference between BSM with heuristic partial slip boundary conditions and BSM-DSMC.

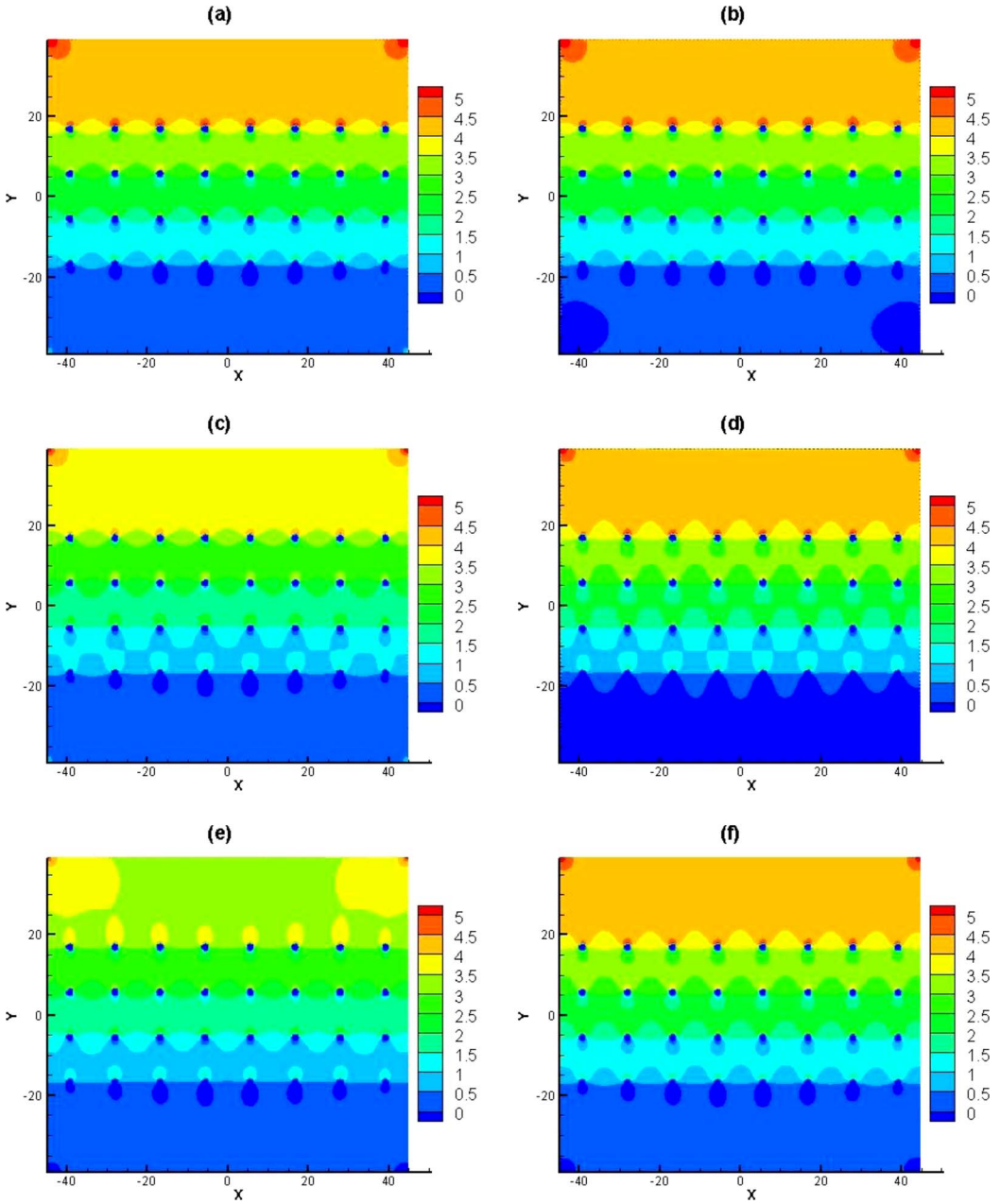

FIG. 11. Pressure isolines for filter with 4 × 8 matrix of fibers: (a), (c), and (e) obtained by the BSM with heuristic slip boundary condition; (b), (d), and (f) obtained by the hybrid BSM and DSMC method; (a), (b), $Kn = 0.1$; (c), (d) $Kn = 0.5$; and (e), (f) $Kn = 1$.

for Stokes flow past a porous body where the external flow is governed by the Stokes equations while the flow through porous body, which occupies only fraction of domain, is computed by DSMC.

B. Numerical results for multi-fiber flows at various Knudsen numbers

The obtained pressure drop (see the beginning of Sec. IV) is presented in Fig. 10 for $Kn = 0.1$, 0.25, 0.5, 0.75, and 1. It is observed that the relative difference between the pressure drop obtained by the BSM and the hybrid method is more prominent at higher Knudsen numbers. For $Kn \leq 0.25$,

the increase in pressure drop between the BSM with heuristic boundary conditions and the hybrid method is less than 10% (see the dashed 10%-line in Fig. 11).

The pressure contours for $Kn = 0.1$, 0.5, and 1.0 are presented in Fig. 11. For $Kn = 0.1$, the pressure contours obtained by the hybrid method and by the BSM are similar. With the increase of the Knudsen number, the difference between the results from the two methods becomes larger (see Figs. 11(c)–11(f)). This finding verify that the BSM combined with the first-order partial-slip boundary conditions could be applied to flows with a Knudsen number up to 0.25. On the contrary, for $Kn \geq 0.75$, the difference in pressure drop is close to 20% (see Fig. 10 and Figs. 11(e) and 11(f)). A study of Poiseuille flow by using both continuum modeling with partial-slip heuristic boundary conditions and molecular method is presented in Ref. 13 to show that the continuum modeling gives a lower shear stress at the wall for higher Knudsen number flows. In turn, this variation in drag affects the pressure drop.

V. CONCLUSIONS

Continuum BSM and the molecular DSMC method are coupled to model filtration flows in the transition molecular-to-continuum regime. The DSMC is applied to the areas surrounding individual fibers while BSM is applied to entire domain. The slip velocity boundary conditions for BSM are computed by DSMC and sampled at the fibers' surface. In turn, boundary conditions for DSMC at the outer boundary of DSMC zone are taken from BSM solution.

For validation purpose, the proposed hybrid BSM-DSMC method is applied to Taylor-Couette flow and to flow about a single fiber confined between two planar walls. The pressure and flow velocity variables are quantified for the range of Knudsen numbers in partial slip and transition regimes.

Parameters of the coupled BSM and DSMC are optimized to ensure numerical accuracy, convergence, and stability with the minimum amount of needed computational resources. The thickness of the DSMC region, the number of simulated particles in DSMC, and the cell size for the DSMC procedure are determined. It is shown that one coupling between the BSM and DSMC is sufficient to obtain accurate numerical results.

The proposed coupled BSM-DSMC is applied to compute flow field in filter with multiple fibers. When the Knudsen number is less than 0.25, the obtained numerical results show less than 10% of difference in pressure drop between the BSM with heuristic partial slip boundary condition and proposed coupled BSM-DSMC method. With the increase in Knudsen number, the difference between results obtained by these two methods becomes more noticeable. If $Kn = 1$, the difference in pressure drop reaches 20% per row. The computed slip flow velocity at fibers' surface differs as much as 3-5 times between coupled BSM-DSMC and BSM with heuristic slip boundary condition. The angular distribution of slip velocity at $Kn = 0.5$ and $Kn = 1$ is significantly more uniform if the coupled BSM-DSMC method is applied. The noticeable difference in magnitude of flow speed between two methods is observed in the fiber mat at distance of up to five radii apart of fibers' surface. This confirms the practical need to account for details of flow slipping layer by using the coupled BSM-DSMC.

[1] R. C. Brown, *Air Filtration: An Integrated Approach to the Theory and Applications of Fibrous Filters* (Pergamon Press, New York, 1993).
[2] V. A. Kirsch, "Stokes flow in model fibrous filters," Sep. Purif. Technol. **58**, 288 (2007).
[3] K. W. Lee and B. Y. H. Liu, "Theoretical study of aerosol filtration by fibrous filters," Aerosol Sci. Technol. **1**, 147 (1982).
[4] C. Zhu, C. H. Lin, and C. S. Cheung, "Inertial impaction-dominated fibrous filtration with rectangular or cylindrical fibers," Powder Technol. **112**, 149 (2000).
[5] S. J. Dunnett and C. F. Clement, "A numerical study of the effects of loading from diffusive deposition on the efficiency of fibrous filters," J. Aerosol Sci. **37**, 1116 (2006).
[6] M. Ouyang and B. Y. H. Liu, "Analytical solution of flow field and pressure drop for filters with rectangular fibers," J. Aerosol Sci. **29**, 187 (1998).
[7] C. Kanaoka, S. Hiragi, and W. Tanthapanichakoon, "Stochastic simulation of the agglomerative deposition process of aerosol particles on an electret fiber," Powder Technol. **118**, 97 (2001).
[8] C. Shin, "Filtration application from recycled expanded polystyrene," J. Colloid Interface Sci. **302**(1), 267 (2006).
[9] Y. Polyakov, "Particle deposition in outside-in hollow fiber filters and its effect on their performance," J. Membr. Sci. **278**(1–2), 190 (2006).

[10] L. R. Huang, E. C. Cox, R. H. Austin, and J. C. Sturm, "Continuous particle separation through deterministic lateral displacement," Science **304**, 987–990 (2004).
[11] A. Jain and J. D. Posner, "Particle dispersion and separation resolution of pinched flow fractionation," Anal. Chem. **80**, 1641–1648 (2008).
[12] W. H. Zhong, I. G. Currie, and D. F. James, "Creeping flow through a model fibrous porous media," Exp. Fluids **40**, 119 (2006).
[13] G. E. Karniadakis and A. Beskok, *Micro Flows: Fundamentals and Simulation* (Springer-Verlag, New York, 2002).
[14] D. L. Young, S. J. Jane, C. M. Fan, K. Murugesan, and C. C. Tsai, "The method of fundamental solutions for 2D and 3D Stokes flows," J. Comput. Phys. **211**, 1 (2006).
[15] H. Zhou and C. Pozrikidis, "Adaptive singularity method for Stokes flow past particles," J. Comput. Phys. **117**, 79 (1995).
[16] T. Götz, "Simulating particles in Stokes flow," J. Comput. Appl. Math. **175**, 415 (2005).
[17] J. Lighthill, "Helical distributions of Stokeslets," J. Eng. Math. **30**, 35 (1996).
[18] R. Cortez, L. Fauci, and A. Medovikov, "The method of regularized Stokeslets in three dimensions: Analysis, validation, and application to helical swimming," Phys. Fluids **17**, 031504 (2005).
[19] W. Wang and K. H. Parker, "Movement of spherical particles in capillaries using a boundary singularity method," J. Biomech. **31**, 347 (1998).
[20] S. Zhao and A. Povitsky, "Boundary singularity method for partial-slip flows," Eng. Anal. Boundary Elem. **35**(1), 114–122 (2011); Preliminary version: AIAA Paper 2007-3989, 2007.
[21] S. Zhao and A. Povitsky, "Method of submerged Stokeslets for slip flow about ensembles of particles," J. Nanosci. Nanotechnol. **8**(7), 3790 (2008).
[22] S. Zhao and A. Povitsky, "Boundary singularity method for partial-slip fibrous filtration flows," Int. J. Numer. Methods Fluids **61**, 255–274 (2009).
[23] M. A. Rieffel, "A method for estimating the computational requirements of DSMC simulations," J. Comput. Phys. **149**, 95 (1999).
[24] G. A. Bird, *Molecular Gas Dynamics and the Direct Simulation of Gas Flows* (Clarendon Press, Oxford, 1994).
[25] F. J. Alexander and A. L. Garcia, "The direct simulation Monte Carlo method," Comput. Phys. **11**, 588 (1997).
[26] G. A. Bird, "Recent advances and current challenges for DSMC," Comput. Math. Appl. **35**, 1 (1998).
[27] F. J. Alexander, A. L. Garcia, and B. J. Alder, "Direct simulation Monte Carlo for thin-film bearings," Phys. Fluids **6**, 3854 (1994).
[28] W. Huang, D. B. Bogy, and A. L. Garcia, "Three-dimensional direct simulation Monte Carlo method for slider air bearings," Phys. Fluids **9**, 1764 (1997).
[29] C. R. Kaplan, J. Liu, and E. S. Oran, "Parallel hybrid method for subsonic flows: Coupling and load-balancing challenges," AIAA Paper 2006-992, 2006.
[30] H. S. Wijesinghe, R. Hornung, A. L. Garcia, and N. G. Hadjiconstantinou, "Three dimensional hybrid continuum-atomistic simulations for multiscale hydrodynamics," J. Fluids Eng. **126**(5), 768 (2004).
[31] O. Aktas and N. R. Aluru, "A combined continuum/DSMC technique for multiscale analysis of microfluidic filters," J. Comput. Phys. **178**, 342 (2002).
[32] R. Roveda, D. B. Goldstein, and P. L. Varghese, "Hybrid Euler/direct simulation Monte Carlo calculation of unsteady slit flow," J. Spacecr. Rockets **37**, 753 (2000).
[33] P. L. Tallec and F. Mallinger, "Coupling Boltzmann and Navier-Stokes equations by half fluxes," J. Comput. Phys. **136**, 51 (1997).
[34] Q. Sun, I. D. Boyd, and G. V. Candler, "A hybrid continuum/particle approach for modeling subsonic, rarefied gas flows," J. Comput. Phys. **194**, 256 (2004).
[35] S. Kim and S. J. Karria, *Microhydrodynamics: Priciples and Selected Applications* (Butterworth-Heinemann, Boston, 1991).
[36] C. Pozrikidis, *Boundary Integral and Singularity Methods for Linearized Viscous Flow* (Cambridge University Press, New York, 1992).
[37] F. J. Alexander, A. L. Garcia, and B. J. Alder, "Cell size dependence of transport coefficients in stochastic particle algorithms," Phys. Fluids **10**(6), 1540 (1998).
[38] F. J. Alexander, A. L. Garcia, and B. J. Alder, "Erratum: "Cell size dependence of transport coefficients in stochastic particle algorithms" [Phys. Fluids **10**, 1540 (1998)]," Phys. Fluids **12**(3), 731 (2000).
[39] N. G. Hadjiconstantinou, "Analysis of discretization in the direct simulation Monte Carlo," Phys. Fluids **12**(10), 2634 (2000).
[40] A. L. Garcia and W. Wagner, "Time step truncation error in direct simulation Monte Carlo," Phys. Fluids **12**(10), 2621 (2000).
[41] P. Y. Tzeng and M. H. Liu, "Influence of number of simulated particles on DSMC modeling of micro-scale Rayleigh-Bénard flows," Int. J. Heat Mass Transfer **48**, 2841 (2005).
[42] G. Chen and I. D. Boyd, "Statistical error analysis for the direct simulation Monte Carlo technique," J. Comput. Phys. **126**, 434 (1996).
[43] N. G. Hadjiconstantinou, A. L. Garcia, M. Z. Bazant, and G. He, "Statistical error in particle simulations of hydrodynamic phenomena," J. Comput. Phys. **187**, 274 (2003).
[44] C. Shen, *Rarefied Gas Dynamics: Fundamentals, Simulations and Micro Flows* (Springer, New York, 2005).
[45] G. Palaniswaamy and S. K. Loyalka, "Direct simulation Monte Carlo aerosol dynamics: Collisional sampling algorithms," Ann. Nucl. Eng. **34**, 13 (2007).
[46] S. Rjasanow and W. Wagner, "On time counting procedures in the DSMC method for rarefied gases," Math. Comput. Simul. **48**, 151 (1998).

[47] E. S. Oran, C. K. Oh, and B. Z. Cybyk, "Direct simulation Monte Carlo: Recent advances and applications," Annu. Rev. Fluid Mech. **30**, 403 (1998).
[48] R. L. Panton, *Incompressible Flow* (John Wiley and Sons, New York, 1984).
[49] N. G. Hadjiconstantinou and A. T. Patera, "Heterogeneous atomistic-continuum representations for dense fluid systems," Int. J. Mod. Phys. C **08**(4), 967–976 (1997).
[50] N. G. Hadjiconstantinou, "Hybrid atomistic-continuum formulations and the moving contact-line problems," J. Comput. Phys. **154**, 245–265 (1999).
[51] T. Werder, J. H. Walther, and P. Koumoutsakos, "Hybrid atomistic-continuum method for the simulation of dense fluid flows," J. Comput. Phys. **205**(1), 373–390 (2005).